Determination of resultant force and moment of light radiation pressure upon a perspective space telescope Millimetron

Mr. Nerovny N.A.[1]
Prof. Zimin V.N.[1]
Dr. Fedorchuk S.D.[2]
Mr. Golubev E.S.[2]

[1] Bauman Moscow State Technical University, nick.nerovny@bmstu.ru
[2] Astro Space Center of P.N. Lebedev Physical Institute

"The Fourth International Symposium on Solar Sailing 2017"
ISSS-2017,
17th – 20th January, Kyoto, JAPAN.

Contents

Research goal

Determination of light radiation pressure upon a space structures with complex geometry.

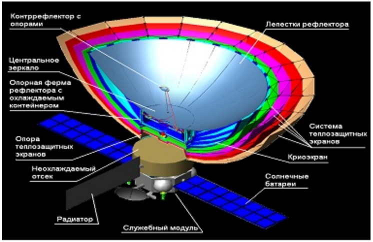

Millimetron / ASC of Physical Institute of RAS

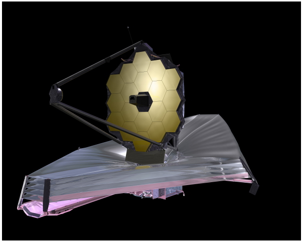

JWST / NASA

$\leftarrow$?

Light pressure

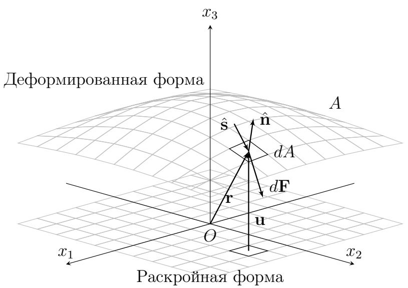

Major assumptions:

- Transmittance is not considered;
- Reflectivity can be both specular or diffuse or both;
- Diffuse reflection can be Lambertian, or other axis-symmetric dispersion law can be considered;
- Temperature is constant in the normal direction;
- The light flux is parallel;
- No self-shadowing and no secondary reflections;
- The structure is optically convex.

The infinitesimal light pressure force

$$d\mathbf{F} = \frac{q_0}{c}\left[-\frac{\varepsilon B \sigma T^4}{q_0}\hat{\mathbf{n}} - (1-\rho s)(\hat{\mathbf{n}}\cdot\hat{\mathbf{s}})\hat{\mathbf{s}} + \rho(1-s)B(\hat{\mathbf{n}}\cdot\hat{\mathbf{s}})\hat{\mathbf{n}} - 2\rho s(\hat{\mathbf{n}}\cdot\hat{\mathbf{s}})^2\hat{\mathbf{n}}\right] dA, \tag{1}$$

after defining of a_0, a_1, a_2, a_3,

$$d\mathbf{F} = P(R)\left[-a_0\hat{\mathbf{n}} - a_1(\hat{\mathbf{n}}\cdot\hat{\mathbf{s}})\hat{\mathbf{s}} + a_2(\hat{\mathbf{n}}\cdot\hat{\mathbf{s}})\hat{\mathbf{n}} - 2a_3(\hat{\mathbf{n}}\cdot\hat{\mathbf{s}})^2\hat{\mathbf{n}}\right] dA. \tag{2}$$

The moment from infinitesimal light pressure force:

$$d\mathbf{M} = \mathbf{r} \times d\mathbf{F}. \tag{3}$$

Let us introduce the visibility function (similar to D.J. Scheeres and L. Rios-Reyes[1]):

$$f(\hat{\mathbf{n}}, \hat{\mathbf{s}}) = \frac{\hat{\mathbf{n}} \cdot \hat{\mathbf{s}} - |\hat{\mathbf{n}} \cdot \hat{\mathbf{s}}|}{2}. \tag{4}$$

Eq. (2) can be rewritten with visibility function:

$$d\mathbf{F} = \frac{P(R)}{2}\Big(- 2a_0\hat{\mathbf{n}} - a_1(\hat{\mathbf{n}} \cdot \hat{\mathbf{s}})\hat{\mathbf{s}} + a_2(\hat{\mathbf{n}} \cdot \hat{\mathbf{s}})\hat{\mathbf{n}} - 2a_3(\hat{\mathbf{n}} \cdot \hat{\mathbf{s}})^2\hat{\mathbf{n}} + a_1|\hat{\mathbf{n}} \cdot \hat{\mathbf{s}}|\hat{\mathbf{s}}$$
$$-a_2|\hat{\mathbf{n}} \cdot \hat{\mathbf{s}}|\hat{\mathbf{n}} + 2a_3(\hat{\mathbf{n}} \cdot \hat{\mathbf{s}})|\hat{\mathbf{n}} \cdot \hat{\mathbf{s}}|\hat{\mathbf{n}}\Big) dA. \tag{5}$$

As far as $\hat{\mathbf{n}} \cdot \hat{\mathbf{s}} \in [-1; 1]$, the $|\hat{\mathbf{n}} \cdot \hat{\mathbf{s}}|$ can be represented as a series of Chebyshev polynomials of the first kind:

$$|\hat{\mathbf{n}} \cdot \hat{\mathbf{s}}| = \frac{2}{\pi} - \frac{4}{\pi}\sum_{n=1}^{\infty}\frac{(-1)^n T_{2n}(\hat{\mathbf{n}} \cdot \hat{\mathbf{s}})}{-1 + 4n^2} =$$
$$= -\frac{4}{\pi}\sum_{n=1}^{\infty}\sum_{k=0}^{n-1}\frac{(-1)^n(-1)^k n(2n-k-1)!}{(-1+4n^2)k!(2n-2k)!}4^{n-k}(\hat{\mathbf{n}} \cdot \hat{\mathbf{s}})^{2(n-k)}. \tag{6}$$

After transformations (6) can be written in simplified form:

$$|\hat{\mathbf{n}} \cdot \hat{\mathbf{s}}| = \sum_{m=1}^{\infty} B_m(\hat{\mathbf{n}} \cdot \hat{\mathbf{s}})^{2m}, \tag{7}$$

where

$$B_m = -\frac{(-1)^m 4^{m+1}}{\pi(2m)!}\sum_{n=m}^{\infty}\frac{n(n+m-1)!}{(-1+4n^2)(n-m)!}. \tag{8}$$

[1] Rios-Reyes, L. and Scheeres, D. J. Generalized Model for Solar Sails, Journal of Spacecraft and Rockets, 42 (1), 2005, pp.182-185.

The series (8) diverge, but in the final summation (7) the divergences are regularized (it can be simply proven since the original series expansion is convergent). We will limit the number of terms in (7) by $N_{\max}$, the upper bound for (8) will be

$$N_{\max B} = \left\lfloor \frac{N_{\max} - 1}{2} \right\rfloor,$$

where $\lfloor x \rfloor$ is a floor function of real x.

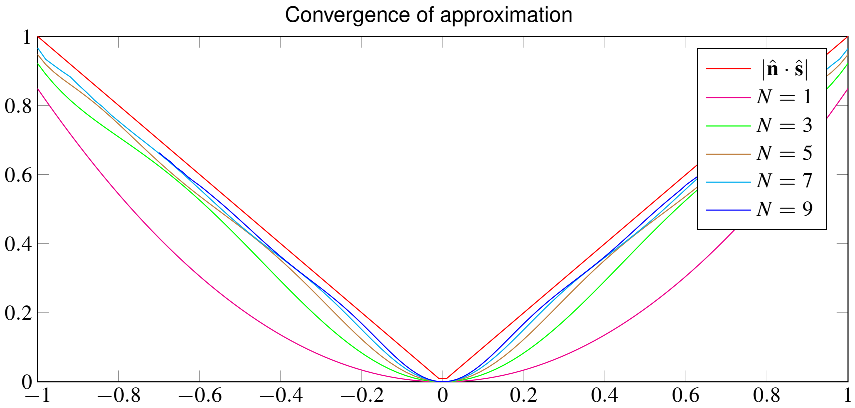

Figure 1: Different approximation rank for $|\hat{\mathbf{n}} \cdot \hat{\mathbf{s}}|$

Let us substitute Eq. (7) into Eq. (5):

$$d\mathbf{F} = \frac{P(R)}{2}\Big(-2a_0\hat{\mathbf{n}} - a_1(\hat{\mathbf{n}}\cdot\hat{\mathbf{s}})\hat{\mathbf{s}} + a_2(\hat{\mathbf{n}}\cdot\hat{\mathbf{s}})\hat{\mathbf{n}} - 2a_3(\hat{\mathbf{n}}\cdot\hat{\mathbf{s}})^2\hat{\mathbf{n}} + a_1\sum_{m=1}^{N_{\max}} B_m(\hat{\mathbf{n}}\cdot\hat{\mathbf{s}})^{2m}\hat{\mathbf{s}} - a_2\sum_{m=1}^{N_{\max}} B_m(\hat{\mathbf{n}}\cdot\hat{\mathbf{s}})^{2m}\hat{\mathbf{n}} + 2a_3\sum_{m=1}^{N_{\max}} B_m(\hat{\mathbf{n}}\cdot\hat{\mathbf{s}})^{2m+1}\hat{\mathbf{n}}\Big)dA. \tag{9}$$

Extending the approach of D.J. Scheeres and others, we can introduce the new shape tensors:

$$\underbrace{(\hat{\mathbf{n}}\cdot\hat{\mathbf{s}})\ldots(\hat{\mathbf{n}}\cdot\hat{\mathbf{s}})}_{p}\,\hat{\mathbf{n}} = (\underbrace{\hat{\mathbf{n}}\otimes\hat{\mathbf{n}}\otimes\ldots\otimes\hat{\mathbf{n}}}_{p+1})\cdot\underbrace{\hat{\mathbf{s}}\cdot\ldots\cdot\hat{\mathbf{s}}}_{p} = \mathcal{J}_A^{p+1}\cdot\underbrace{\hat{\mathbf{s}}\cdot\ldots\cdot\hat{\mathbf{s}}}_{p};$$

$$\underbrace{(\hat{\mathbf{n}}\cdot\hat{\mathbf{s}})\ldots(\hat{\mathbf{n}}\cdot\hat{\mathbf{s}})}_{p}\,\hat{\mathbf{s}} = (\underbrace{\hat{\mathbf{n}}\otimes\hat{\mathbf{n}}\otimes\ldots\otimes\hat{\mathbf{n}}}_{p}\otimes\mathcal{E}^2)\cdot\underbrace{\hat{\mathbf{s}}\cdot\ldots\cdot\hat{\mathbf{s}}}_{p+1} = \mathcal{J}_B^{p+2}\cdot\underbrace{\hat{\mathbf{s}}\cdot\ldots\cdot\hat{\mathbf{s}}}_{p+1}.$$

After rewriting of Eq. (9) in the tensor notation:

$$d\mathbf{F} = \frac{P(R)}{2}\Big(-2a_0\hat{\mathbf{n}} - a_1\mathcal{J}_B^3\cdot\hat{\mathbf{s}}\cdot\hat{\mathbf{s}} + a_2\mathcal{J}_A^2\cdot\hat{\mathbf{s}} - 2a_3\mathcal{J}_A^3\cdot\hat{\mathbf{s}}\cdot\hat{\mathbf{s}} + a_1\sum_{m=1}^{N_{\max}} B_m\mathcal{J}_B^{2m+2}\cdot\underbrace{\hat{\mathbf{s}}\cdot\ldots\cdot\hat{\mathbf{s}}}_{2m+1} - a_2\sum_{m=1}^{N_{\max}} B_m\mathcal{J}_A^{2m+1}\cdot\underbrace{\hat{\mathbf{s}}\cdot\ldots\cdot\hat{\mathbf{s}}}_{2m} + 2a_3\sum_{m=1}^{N_{\max}} B_m\mathcal{J}_A^{2m+2}\cdot\underbrace{\hat{\mathbf{s}}\cdot\ldots\cdot\hat{\mathbf{s}}}_{2m+1}\Big)dA. \tag{10}$$

By grouping of terms in (10) we can write the equation for infinitesimal force of light pressure falling only to the front side:

$$d\mathbf{F} = P(R)\left(\mathcal{J}^1 + \sum_{n=2}^{N_{\max}} \mathcal{J}^n \cdot \underbrace{\hat{\mathbf{s}} \cdot \ldots \cdot \hat{\mathbf{s}}}_{n-1}\right) dA, \tag{11}$$

where

$$\mathcal{J}^1 = -a_0 \hat{\mathbf{n}}; \tag{12}$$

$$\mathcal{J}^2 = \frac{1}{2} a_2 \mathcal{J}_A^2; \tag{13}$$

$$\mathcal{J}^3 = \frac{1}{2}\left(-a_1 \mathcal{J}_B^3 - 2a_3 \mathcal{J}_A^3 - B_1 a_2 \mathcal{J}_A^3 \right); \tag{14}$$

$$\mathcal{J}^n = \frac{1}{2}\left(-B_{\frac{n-1}{2}} \frac{1-(-1)^n}{2} a_2 \mathcal{J}_A^n + B_{\frac{n-2}{2}} \frac{1+(-1)^n}{2} \left(a_1 \mathcal{J}_B^n + 2a_3 \mathcal{J}_A^n\right) \right), \ n > 3; \tag{15}$$

$$\mathcal{J}_A^n = \underbrace{\hat{\mathbf{n}} \otimes \ldots \otimes \hat{\mathbf{n}}}_{n}; \tag{16}$$

$$\mathcal{J}_B^n = \underbrace{\hat{\mathbf{n}} \otimes \ldots \otimes \hat{\mathbf{n}}}_{n-2} \otimes \mathcal{E}^2. \tag{17}$$

Providing the same procedure for the moment:

$$\underbrace{(\hat{\mathbf{n}}\cdot\hat{\mathbf{s}})\dots(\hat{\mathbf{n}}\cdot\hat{\mathbf{s}})}_{p}(\mathcal{R}^2\cdot\hat{\mathbf{n}}) = (\underbrace{\hat{\mathbf{n}}\otimes\hat{\mathbf{n}}\otimes\dots\otimes\hat{\mathbf{n}}}_{p}\otimes\mathcal{R}^2\cdot\hat{\mathbf{n}})\cdot\underbrace{\hat{\mathbf{s}}\cdot\dots\cdot\hat{\mathbf{s}}}_{p} = \mathcal{L}_A^{p+1}\cdot\underbrace{\hat{\mathbf{s}}\cdot\dots\cdot\hat{\mathbf{s}}}_{p};$$

$$\underbrace{(\hat{\mathbf{n}}\cdot\hat{\mathbf{s}})\dots(\hat{\mathbf{n}}\cdot\hat{\mathbf{s}})}_{p}(\mathcal{R}^2\cdot\hat{\mathbf{s}}) = (\underbrace{\hat{\mathbf{n}}\otimes\hat{\mathbf{n}}\otimes\dots\otimes\hat{\mathbf{n}}}_{p}\otimes\mathcal{R}^2)\cdot\underbrace{\hat{\mathbf{s}}\cdot\dots\cdot\hat{\mathbf{s}}}_{p+1} = \mathcal{L}_B^{p+2}\cdot\underbrace{\hat{\mathbf{s}}\cdot\dots\cdot\hat{\mathbf{s}}}_{p+1},$$

we can also represent the Eq. (9) as a tensor series:

$$d\mathbf{M} = \mathbf{r}\times d\mathbf{F} = \mathcal{R}^2\cdot d\mathbf{F} = \frac{P(R)}{2}\Bigg(-2a_0\mathcal{R}^2\cdot\hat{\mathbf{n}} - a_1\mathcal{L}_B^3\cdot\hat{\mathbf{s}}\cdot\hat{\mathbf{s}} + a_2\mathcal{L}_A^2\cdot\hat{\mathbf{s}} - 2a_3\mathcal{L}_A^3\cdot\hat{\mathbf{s}}\cdot\hat{\mathbf{s}} + a_1\sum_{m=1}^{N_{\max}} B_m\mathcal{L}_B^{2m+2}\cdot\underbrace{\hat{\mathbf{s}}\cdot\dots\cdot\hat{\mathbf{s}}}_{2m+1} - a_2\sum_{m=1}^{N_{\max}} B_m\mathcal{L}_A^{2m+1}\cdot\underbrace{\hat{\mathbf{s}}\cdot\dots\cdot\hat{\mathbf{s}}}_{2m} + 2a_3\sum_{m=1}^{N_{\max}} B_m\mathcal{L}_A^{2m+2}\cdot\underbrace{\hat{\mathbf{s}}\cdot\dots\cdot\hat{\mathbf{s}}}_{2m+1}\Bigg)dA, \tag{18}$$

where

$$\mathcal{L}_A^n = \underbrace{\hat{\mathbf{n}}\otimes\dots\otimes\hat{\mathbf{n}}}_{n-1}\otimes\mathcal{R}^2\cdot\hat{\mathbf{n}}; \tag{19}$$

$$\mathcal{L}_B^n = \underbrace{\hat{\mathbf{n}}\otimes\dots\otimes\hat{\mathbf{n}}}_{n-2}\otimes\mathcal{R}^2. \tag{20}$$

The tensor series for $\mathbf{M}$ will be as the follows:

$$d\mathbf{M} = P(R)\left(\mathcal{L}^1 + \sum_{n=2}^{N_{\max}} \mathcal{L}^n \cdot \underbrace{\hat{\mathbf{s}} \cdot \ldots \cdot \hat{\mathbf{s}}}_{n-1}\right) dA, \tag{21}$$

where

$$\mathcal{L}^1 = -a_0(\mathcal{R}^2 \cdot \hat{\mathbf{n}}); \tag{22}$$

$$\mathcal{L}^2 = \frac{1}{2} a_2 \mathcal{L}_A^2; \tag{23}$$

$$\mathcal{L}^3 = \frac{1}{2}\left(- a_1 \mathcal{L}_B^3 - 2a_3 \mathcal{L}_A^3 - B_1 a_2 \mathcal{L}_A^3 \right); \tag{24}$$

$$\mathcal{L}^n = \frac{1}{2}\left(- B_{\frac{n-1}{2}} \frac{1-(-1)^n}{2} a_2 \mathcal{L}_A^n + B_{\frac{n-2}{2}} \frac{1+(-1)^n}{2} \left(a_1 \mathcal{L}_B^n + 2a_3 \mathcal{L}_A^n\right) \right), \ n > 3; \tag{25}$$

Resulting equation

By integrating of (11) and (21) over the whole surface A, we can get the resultant force and moment upon an optically convex structure:

$$\mathbf{F} = P(R)\left(\tilde{\mathcal{I}}^1 + \sum_{n=2}^{N_{\max}} \tilde{\mathcal{I}}^n \cdot \underbrace{\hat{\mathbf{s}} \cdot \ldots \cdot \hat{\mathbf{s}}}_{n-1}\right); \tag{26}$$

$$\mathbf{M} = P(R)\left(\tilde{\mathcal{K}}^1 + \sum_{n=2}^{N_{\max}} \tilde{\mathcal{K}}^n \cdot \underbrace{\hat{\mathbf{s}} \cdot \ldots \cdot \hat{\mathbf{s}}}_{n-1}\right), \tag{27}$$

where

$$\tilde{\mathcal{I}}^n = \int\limits_A \tilde{\mathcal{J}}^n dA; \tag{28}$$

$$\tilde{\mathcal{K}}^n = \int\limits_A \tilde{\mathcal{L}}^n dA, \tag{29}$$

where $n \geqslant 1$.
It is possible to write the same relations considering self-shadowing and secondary reflections[2].

[2]Nerovny, N.A. et al. Representation of light pressure resultant force and moment as a tensor series // Celestial Mechanics and Dynamical Astronomy. [Approved for publication]

Analytical examples

Assumptions

In the analytical examples below the light source orientation vector $\hat{\mathbf{s}}$ is defined by two angles α and β as follows:

- $\alpha \in [0, 2\pi]$ — angle between unit vector $\hat{\mathbf{e}}_1$ of axis Ox_1 and projection of vector $\hat{\mathbf{s}}$ on the plane Ox_1x_3;
- $\beta \in [-\frac{\pi}{2}; \frac{\pi}{2}]$ — angle between plane Ox_1x_3 and vector $\hat{\mathbf{s}}$.

The components of vector $\hat{\mathbf{s}}$ can be written as follows:

$$\hat{\mathbf{s}} = (\cos\alpha\cos\beta, \sin\beta, \sin\alpha\cos\beta)^T.$$

Flat sail

The front side (side 1) has reflection coefficient ρ_1 and specularity parameter s_1. The other side (side 2) has reflectivity ρ_2 and specularity s_2. The area of the solar sail is A.
Components of tensors $\mathcal{I}$ and $\mathcal{K}$:

$$\mathcal{I} = A\left(\mathcal{J}(\hat{\mathbf{n}}_1, \rho_1, s_1) + \mathcal{J}(\hat{\mathbf{n}}_2, \rho_2, s_2)\right);$$
$$\mathcal{K} = A\left(\mathcal{L}(\hat{\mathbf{n}}_1, \mathbf{r}_1, \rho_1, s_1) + \mathcal{L}(\hat{\mathbf{n}}_2, \mathbf{r}_2, \rho_2, s_2)\right);$$
$$\hat{\mathbf{n}}_1 = (0,0,1)^T;$$
$$\hat{\mathbf{n}}_2 = (0,0,-1)^T;$$
$$\mathbf{r}_1 = \mathbf{r}_2 = (0,0,0)^T.$$

Resultant force and moment ($N_{\max} = 6$):

$$F_1 = \frac{P(R)A}{30\pi}\left(-6(-2+\rho_1 s_1+\rho_2 s_2) + \cos\beta\sin\alpha\left(15\pi(\rho_1 s_1 - \rho_2 s_2) + \right.\right.$$
$$\left.\left. +8(-2+\rho_1 s_1+\rho_2 s_2)\cos\beta\sin\alpha\left(-9+4\cos^2\beta\sin^2\alpha\right)\right)\right)\cos\alpha\cos\beta;$$

$$F_2 = \frac{P(R)A}{30\pi}\left(-6(-2+\rho_1 s_1+\rho_2 s_2) + \cos\beta\sin\alpha\left(15\pi(\rho_1 s_1 - \rho_2 s_2) + \right.\right.$$
$$\left.\left. +8(-2+\rho_1 s_1+\rho_2 s_2)\cos\beta\sin\alpha\left(-9+4\cos^2\beta\sin^2\alpha\right)\right)\right)\sin\beta;$$

$$F_3 = \frac{P(R)A}{90\pi}\left(24(\rho_2(1-s_2) - \rho_1(1-s_1)) + \cos\beta\sin\alpha\right.$$
$$(6(5\pi(\rho_1(1-s_1) + \rho_2(1-s_2)) + 3(2+\rho_1 s_1 \rho_2 s_2)) + \cos\beta\sin\alpha$$
$$(-9(16\rho_1(1-s_1) + 5\pi\rho_1 s_1 - 16\rho_2(1-s_2) - 5\pi\rho_2 s_2) + 8\cos\beta\sin\alpha$$
$$(27(2+\rho_1 s_1+\rho_2 s_2) + 4\cos\beta\sin\alpha(2(\rho_1(1-s_1) - \rho_2(1-s_2)) -$$
$$\left. -3(2+\rho_1 s_2 + \rho_2 s_2)\cos\beta\sin\alpha)))\right);$$

$$\mathbf{M} = 0.$$

Flat solar sail, $N_{\max} = 6$, $\rho_1 = 1,\ \rho_2 = 0,\ s_1 = s_2 = 1$

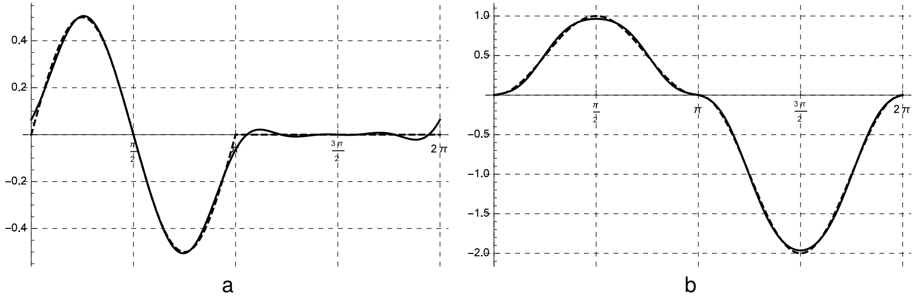

Figure 2: Projection on Ox_1 (a) and on Ox_3 (b) of resultant force of light pressure upon two-sided specular solar sail with unit area, $N_{\max} = 6,\ \rho_1 = 1,\ \rho_2 = 0,\ s_1 = s_2 = 1$. Solid line – approximate solution, dashed line — exact solution. Values are divided by $P(R)$.

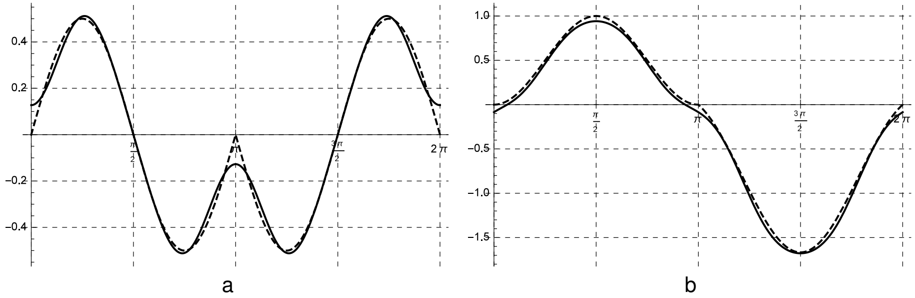

Figure 3: Projection on Ox_1 (a) and on Ox_3 (b) of resultant force of light pressure upon two-sided diffuse solar sail with unit area, $N_{\max} = 6$, $\rho_1 = 1$, $\rho_2 = 0$, $s_1 = s_2 = 0$. Solid line – approximate solution, dashed line – exact solution. Values are divided by $P(R)$.

Let us consider a sphere of radius R_0 with a homogeneous specular-diffusive surface, the reflection coefficient of which is equal to ρ and the degree of specular reflection is s.
The expressions for the components of tensors $\mathcal{I}$ and $\mathcal{K}$:

$$\mathcal{I} = R_0^2 \int_0^{2\pi} \int_{-\frac{\pi}{2}}^{\frac{\pi}{2}} \mathcal{J}(\hat{\mathbf{n}}, \rho, s) d\theta d\phi;$$

$$\mathcal{K} = R_0^2 \int_0^{2\pi} \int_{-\frac{\pi}{2}}^{\frac{\pi}{2}} \mathcal{L}(\hat{\mathbf{n}}, \mathbf{r}, \rho, s) d\theta d\phi;$$

$$\hat{\mathbf{n}} = (\cos\phi\cos\theta, \sin\phi\cos\theta, \sin\theta)^T;$$

$$\mathbf{r} = (R_0\cos\phi\cos\theta, R_0\sin\phi\cos\theta, R_0\sin\theta)^T.$$

The analytical expressions considering $N_{\max} = 6$:

$$F_1 = P(R)\frac{4}{1575}\left(175\pi\rho(1-s) + 3(413+\rho s)\right) R_0^2 \cos\alpha\cos\beta;$$

$$F_2 = P(R)\frac{4}{1575}\left(175\pi\rho(1-s) + 3(413+\rho s)\right) R_0^2 \sin\beta;$$

$$F_3 = P(R)\frac{4}{1575}\left(175\pi\rho(1-s) + 3(413+\rho s)\right) R_0^2 \cos\beta\sin\alpha;$$

$$\mathbf{M} = 0.$$

Ideally specular sphere

For $\rho = 1$ and $s = 1$ we get:

$$F_1 \approx P(R)\pi R_0^2 \cos\alpha \cos\beta; \tag{30}$$

$$F_2 \approx P(R)\pi R_0^2 \sin\beta; \tag{31}$$

$$F_3 \approx P(R)\pi R_0^2 \cos\beta \sin\alpha. \tag{32}$$

Let us consider the cylinder with following parameters:

- ρ_0 — reflectance of the envelope;
- ρ_1 — reflectance of the butt surface $+x_3$;
- ρ_2 — reflectance of the butt surface $-x_3$;
- s_0 — specularity coefficient of the envelope;
- s_1 — specularity coefficient of the butt surface $+x_3$;
- s_2 — specularity coefficient of the butt surface $-x_3$;
- R_1 — radius of the cylinder;
- H — height of the cylinder.

The expressions for the components of tensors $\mathcal{I}$ and $\mathcal{K}$:

$$\mathcal{I} = \mathcal{J}(\hat{\mathbf{n}}_1, \rho_1, s_1)\pi R_1^2 + \mathcal{J}(\hat{\mathbf{n}}_2, \rho_2, s_2)\pi R_1^2 + HR_1 \int\limits_0^{2\pi} \mathcal{J}(\hat{\mathbf{n}}_0, \rho_0, s_0)d\phi;$$

$$\mathcal{K} = \mathcal{L}(\hat{\mathbf{n}}_1, \mathbf{r}_1, \rho_1, s_1)\pi R_1^2 + \mathcal{L}(\hat{\mathbf{n}}_2, \mathbf{r}_2, \rho_2, s_2)\pi R_1^2 + HR_1 \int\limits_0^{2\pi} \mathcal{L}(\hat{\mathbf{n}}_0, \mathbf{r}_0, \rho_0, s_0)d\phi;$$

$$\begin{aligned}
\hat{\mathbf{n}}_1 &= (0, 0, 1)^T; \\
\hat{\mathbf{n}}_2 &= (0, 0, -1)^T; \\
\hat{\mathbf{n}}_0 &= (\cos\phi, \sin\phi, 0)^T; \\
\mathbf{r}_1 &= (0, 0, H/2)^T; \\
\mathbf{r}_2 &= (0, 0, -H/2)^T; \\
\mathbf{r}_0 &= (R_1\cos\phi, R_1\sin\phi, 0)^T.
\end{aligned}$$

For the number of terms of the series $N_{\max} = 6$ we can get:

$$
\begin{aligned}
F_1 = {} & \frac{P(R)R_1}{30} \cos\alpha \cos\beta(-8H(3 + 2\rho_0 s_0) \cos^4\alpha \cos^4\beta + \\
& + 4H \cos^2\alpha \cos^2\beta(12 + 5\rho_0 s_0 + (6 + 4\rho_0 s_0) \cos 2\beta) + \\
& + R_1 \cos\beta \sin\alpha(15\pi(\rho_1 s_1 - \rho_2 s_2) + \\
& + 8(-2 + \rho_1 s_1 + \rho_2 s_2) \cos\beta \sin\alpha(-9 + 4\cos^2\beta \sin^2\alpha)) + \\
& + 2(H(6 - 5\pi\rho_0(-1 + s_0)) - 3R_1(-2 + \rho_1 s_1 + \rho_2 s_2) + \\
& + 2H(15 + 7\rho_0 s_0 + (3 + 2\rho_0 s_0) \cos 2\beta) \sin^2\beta)); \\
F_2 = {} & \frac{P(R)R_1}{30} \sin\beta(-8H(3 + 2\rho_0 s_0) \cos^4\alpha \cos^4\beta + \\
& + 4H \cos^2\alpha \cos^2\beta(12 + 5\rho_0 s_0 + (6 + 4\rho_0 s_0) \cos 2\beta) + \\
& + R_1 \cos\beta \sin\alpha(15\pi(\rho_1 s_1 - \rho_2 s_2) + \\
& + 8(-2 + \rho_1 s_1 + \rho_2 s_2) \cos\beta \sin\alpha(-9 + 4\cos^2\beta \sin^2\alpha)) + \\
& + 2(H(6 - 5\pi\rho_0(-1 + s_0)) - 3R_1(-2 + \rho_1 s_1 + \rho_2 s_2) + \\
& + 2H(15 + 7\rho_0 s_0 + (3 + 2\rho_0 s_0) \cos 2\beta) \sin^2\beta));
\end{aligned}
$$

$$F_3 = \frac{P(R)R_1}{90}(24R_1(\rho_2(1-s_2)-\rho_1(1-s_1))+$$
$$+\frac{3}{8}\cos\beta(-363H(-1+\rho_0 s_0)+16R_1(5\pi(\rho_1+\rho_2-\rho_1 s_1-\rho_2 s_2)+$$
$$+3(2+\rho_1 s_1+\rho_2 s_2))+3H(-1+\rho_0 s_0)(44\cos 2\beta+5\cos 4\beta))\sin\alpha-$$
$$-9R_1(\rho_1(16+(-16+5\pi)s_1)+16\rho_2(-1+s_2)-5\pi\rho_2 s_2)\cos^2\beta\sin^2\alpha+$$
$$+64R_1(\rho_1-\rho_1 s_1+\rho_2(-1+s_2))\cos^4\beta\sin^4\alpha+$$
$$+\frac{9}{4}\cos^3\beta(96R_1(2+\rho_1 s_1+\rho_2 s_2)\sin^3\alpha-H(-1+\rho_0 s_0)(13+5\cos 2\beta)\sin 3\alpha)+$$
$$+\frac{3}{2}\cos^5\beta(-64R_1(2+\rho_1 s_1+\rho_2 s_2)\sin^5\alpha+3H(-1+\rho_0 s_0)\sin 5\alpha));$$
$$M_1 = \frac{P(R)HR_1^2}{60}(6\rho_1 s_1-6\rho_2 s_2+\cos\beta\sin\alpha(15\pi(-2\rho_0 s_0+\rho_1 s_1+\rho_2 s_2)+$$
$$+8(\rho_1 s_1-\rho_2 s_2)\cos\beta\sin\alpha(-9+4\cos^2\beta\sin^2\alpha)))\sin\beta;$$
$$M_2 = \frac{P(R)HR_1^2}{60}(-6\rho_1 s_1+6\rho_2 s_2+\cos\beta\sin\alpha(15\pi(2\rho_0 s_0-\rho_1 s_1-\rho_2 s_2)+$$
$$+8(\rho_1 s_1-\rho_2 s_2)\cos\beta\sin\alpha(9-4\cos^2\beta\sin^2\alpha)))\cos\alpha\cos\beta;$$
$$M_3 = 0.$$

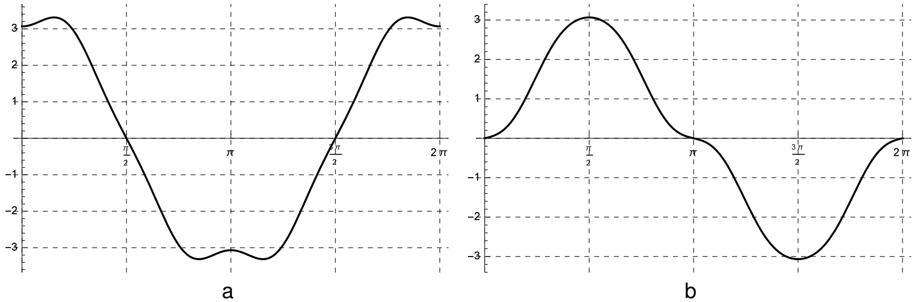

Figure 4: Projection on Ox_1 (a) and on Ox_3 (b) of resultant force of light pressure upon specular-diffuse cylinder, $N_{\max} = 6$, $\rho_1 = \rho_2 = 0$, $\rho_0 = 1$, $s_1 = s_2 = 0$, $s_0 = 1$. Values are divided by $P(R)$.

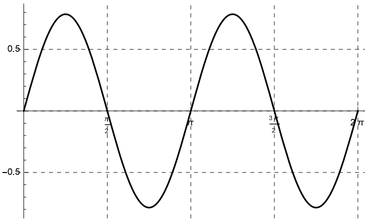

Figure 5: Projection on Ox_2 of principal moment of light pressure upon specular-diffuse cylinder, $N_{\max} = 6$, $\rho_1 = \rho_2 = 0$, $\rho_0 = 1$, $s_1 = s_2 = 0$, $s_0 = 1$. Values are divided by $P(R)$.

Numerical method

Main idea: approximation of shape tensor components using known values of force $\mathbf{f}^{(i)} = \mathbf{F}^{(i)}/P(R)$ and moment $\mathbf{m}^{(i)} = \mathbf{M}^{(i)}/P(R)$ for the set of known orientation vector $\hat{\mathbf{s}}^{(i)}$ in a number N.
The approximated values for shape tensors components $\tilde{\mathcal{I}}^n$ and $\tilde{\mathcal{K}}^n$:

$$\underset{\left[\left(\frac{3}{2}(3^M-1)\right)\times 1\right]}{\mathbf{j}} = \left(\tilde{I}_1^1 \tilde{I}_{11}^2 \tilde{I}_{21}^2 \tilde{I}_{31}^2 \tilde{I}_{111}^3 \ldots \tilde{I}^M_{\underbrace{3\ldots3}_{M-1}1} \tilde{I}_2^1 \ldots \tilde{I}^M_{\underbrace{3\ldots3}_{M-1}2} \tilde{I}_3^1 \ldots \tilde{I}^M_{\underbrace{3\ldots3}_{M}}\right)^T ; \tag{33}$$

$$\underset{\left[\left(\frac{3}{2}(3^M-1)\right)\times 1\right]}{\mathbf{k}} = \left(\tilde{K}_1^1 \tilde{K}_{11}^2 \tilde{K}_{21}^2 \tilde{K}_{31}^2 \tilde{K}_{111}^3 \ldots \tilde{K}^M_{\underbrace{3\ldots3}_{M-1}1} \tilde{K}_2^1 \ldots \tilde{K}^M_{\underbrace{3\ldots3}_{M-1}2} \tilde{K}_3^1 \ldots \tilde{K}^M_{\underbrace{3\ldots3}_{M}}\right)^T , \tag{34}$$

where $M = N_{\max}$.
Vector of free terms:

$$\underset{[3N\times 1]}{\mathbf{f}} = \left(f_1^{(1)} f_1^{(2)} \ldots f_1^{(N)} f_2^{(1)} f_2^{(2)} \ldots f_2^{(N)} f_3^{(1)} f_3^{(2)} \ldots f_3^{(N)}\right)^T ; \tag{35}$$

$$\underset{[3N\times 1]}{\mathbf{m}} = \left(m_1^{(1)} m_1^{(2)} \ldots m_1^{(N)} m_2^{(1)} m_2^{(2)} \ldots m_2^{(N)} m_3^{(1)} m_3^{(2)} \ldots m_3^{(N)}\right)^T . \tag{36}$$

Matrix of orientations:

$$\underset{\left[3n\times\left(\frac{3}{2}(3^M-1)\right)\right]}{S} =$$

$$
\begin{pmatrix}
1 & \cdots & 1 & 0 & \cdots & 0 & 0 & \cdots & 0 \\
s_1^{(1)} & & s_1^{(N)} & & & & & & \\
s_2^{(1)} & & s_2^{(N)} & & & & & & \\
s_3^{(1)} & & s_3^{(N)} & \vdots & & \vdots & \vdots & & \vdots \\
s_1^{(1)} s_1^{(1)} & & s_1^{(N)} s_1^{(N)} & & & & & & \\
\vdots & & \vdots & & & & & & \\
\underbrace{s_3^{(1)} \dots s_3^{(1)}}_{M-1} & \cdots & \underbrace{s_3^{(N)} \dots s_3^{(N)}}_{M-1} & 0 & \cdots & 0 & 0 & \cdots & 0 \\
0 & \cdots & 0 & 1 & \cdots & 1 & 0 & \cdots & 0 \\
& & & s_1^{(1)} & & s_1^{(N)} & & & \\
& & & s_2^{(1)} & & s_2^{(N)} & & & \\
\vdots & & \vdots & s_3^{(1)} & & s_3^{(N)} & \vdots & & \vdots \\
& & & s_1^{(1)} s_1^{(1)} & & s_1^{(N)} s_1^{(N)} & & & \\
& & & \vdots & & \vdots & & & \\
0 & \cdots & 0 & \underbrace{s_3^{(1)} \dots s_3^{(1)}}_{M-1} & \cdots & \underbrace{s_3^{(N)} \dots s_3^{(N)}}_{M-1} & 0 & \cdots & 0 \\
0 & \cdots & 0 & 0 & \cdots & 0 & 1 & \cdots & 1 \\
& & & & & & s_1^{(1)} & & s_1^{(N)} \\
& & & & & & s_2^{(1)} & & s_2^{(N)} \\
\vdots & & \vdots & \vdots & & \vdots & s_3^{(1)} & & s_3^{(N)} \\
& & & & & & s_1^{(1)} s_1^{(1)} & & s_1^{(N)} s_1^{(N)} \\
& & & & & & \vdots & & \vdots \\
0 & \cdots & 0 & 0 & \cdots & 0 & \underbrace{s_3^{(1)} \dots s_3^{(1)}}_{M-1} & \cdots & \underbrace{s_3^{(N)} \dots s_3^{(N)}}_{M-1}
\end{pmatrix}^T .
$$

The resolving equation for $\mathbf{f}$ and $\mathbf{m}$ are overdefined:

$$S\mathbf{j} = \mathbf{f}; \tag{38}$$

$$S\mathbf{k} = \mathbf{m}. \tag{39}$$

$\mathbf{j}$ and $\mathbf{k}$ are approximated by $\tilde{\mathbf{j}}$ and $\tilde{\mathbf{k}}$ using least squares method:

$$||S\mathbf{j} - \mathbf{f}||^2 \to \min, \ \tilde{\mathbf{j}} = \left(S^T S\right)^+ S^T \mathbf{f}; \tag{40}$$

$$||S\mathbf{k} - \mathbf{m}||^2 \to \min, \ \tilde{\mathbf{k}} = \left(S^T S\right)^+ S^T \mathbf{m}, \tag{41}$$

where $^+$ is a pseudo-inverse operator.

Model spacecraft

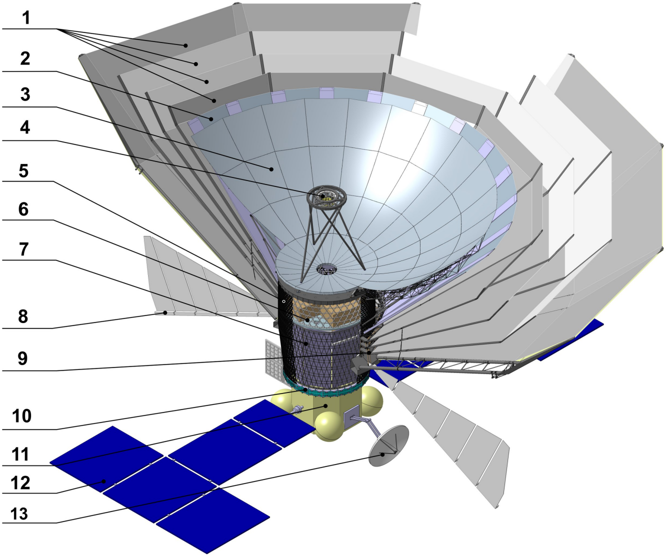

Figure 6: Millimentron space observatory concept. 1 – Sun shields; 2 – Cryo-shield; 3 – Primary mirror's petal; 4 – Secondary mirror; 5 – Central part of Primary mirror; 6 – Cryo-container; 7 – Heat exchanger (radiator); 8 – Warm container; 9 – Sunshields supporting truss; 10 – Adapter ring; 11 – Service module; 12 – Solar power array; 13 – High gain antenna.

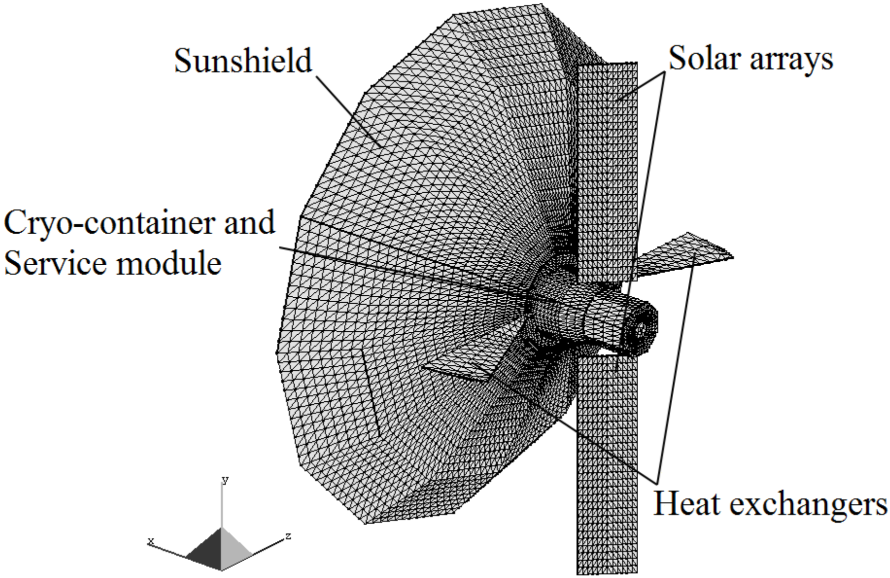

Figure 7: Geometrical model of Millimetron space observatory.

Raytracing results, specular and diffuse cases (1000000 rays), Tracer[3]

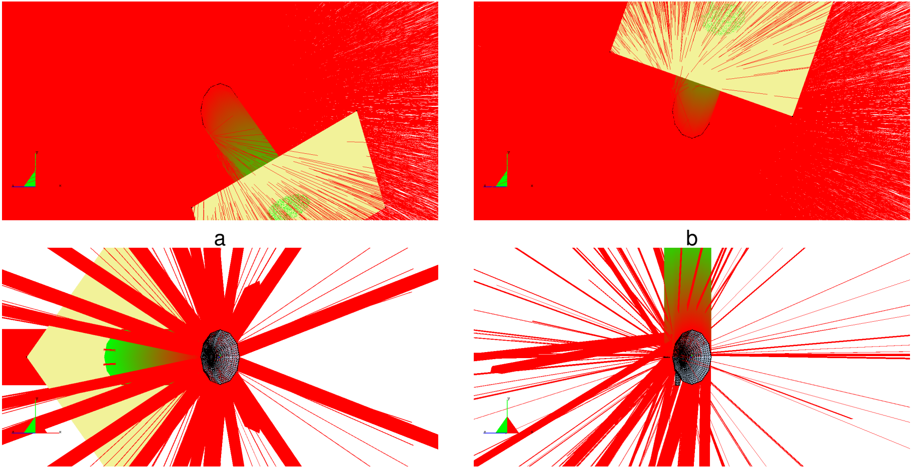

a, b — diffuse cases; c, d — specular cases.

[3] Leonov, V.V. Radiation heat transfer in mirror concentrator systems, PhD Thesis, 2012 (in Russian).

Specular case

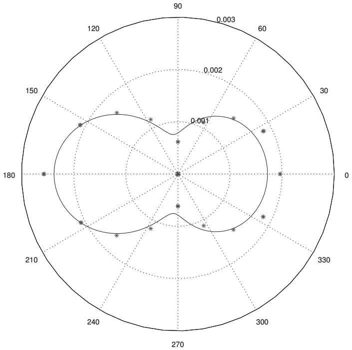

a

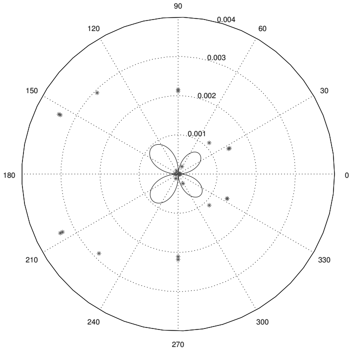

b

Figure 8: Dependency of the absolute value of resultant force and moment of light radiation pressure from the angle of rotation of light source in the radiators plane. Solid line – tensor approximation ($N_{\max} = 2$), dots – Monte–Carlo simulation results which were not used for the approximation. Figure a – absolute value of resultant force, N; Figure b – absolute value of the resultant moment, $N \cdot m$. The whole surface is specular.

Specular case, absolute values, $N_{\max} = 3$

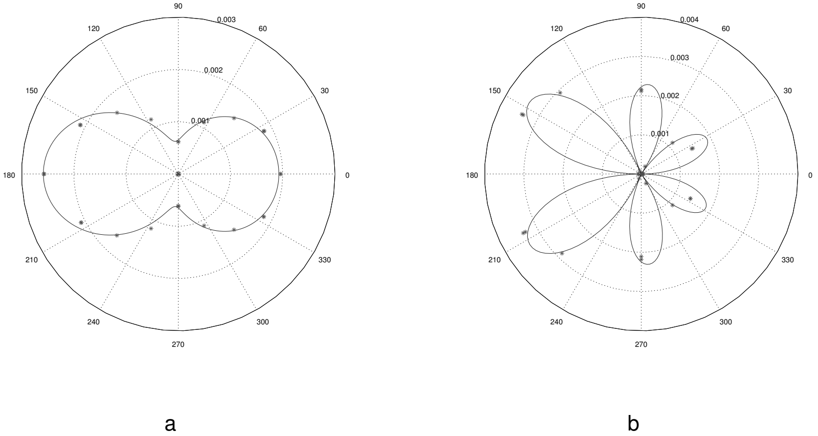

Figure 9: Dependency of the absolute value of resultant force and moment of light radiation pressure from the angle of rotation of light source in the radiators plane. Solid line – tensor approximation ($N_{\max} = 3$), dots – Monte–Carlo simulation results which were not used for the approximation. Figure a – absolute value of resultant force, N; Figure b – absolute value of the resultant moment, $N \cdot m$. The whole surface is specular.

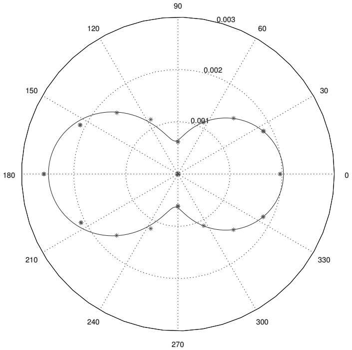

a

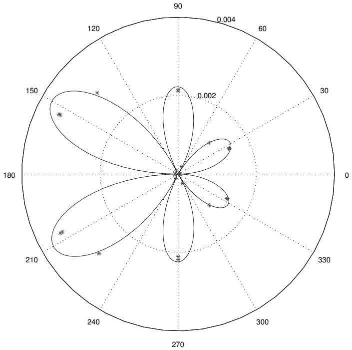

b

Figure 10: Dependency of the absolute value of resultant force and moment of light radiation pressure from the angle of rotation of light source in the radiators plane. Solid line – tensor approximation ($N_{\max} = 4$), dots – Monte–Carlo simulation results which were not used for the approximation. Figure a – absolute value of resultant force, N; Figure b – absolute value of the resultant moment, $N \cdot m$. The whole surface is specular.

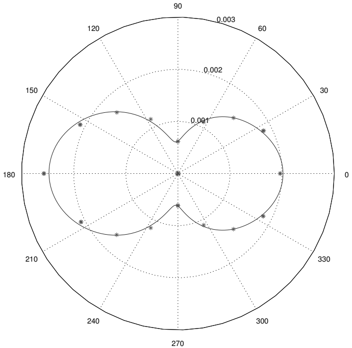

a

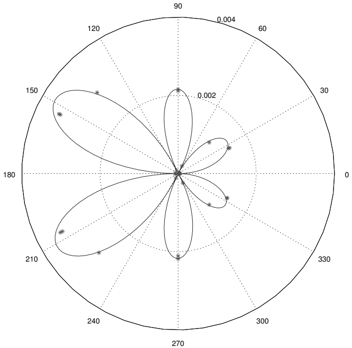

b

Figure 11: Dependency of the absolute value of resultant force and moment of light radiation pressure from the angle of rotation of light source in the radiators plane. Solid line – tensor approximation ($N_{\max} = 5$), dots – Monte–Carlo simulation results which were not used for the approximation. Figure a – absolute value of resultant force, N; Figure b – absolute value of the resultant moment, $N \cdot m$. The whole surface is specular.

Specular case, absolute values, $N_{\max} = 6$

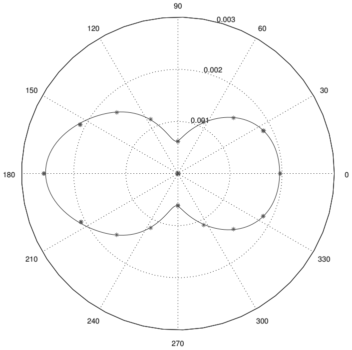

a

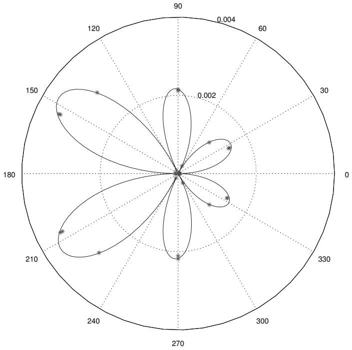

b

Figure 12: Dependency of the absolute value of resultant force and moment of light radiation pressure from the angle of rotation of light source in the radiators plane. Solid line – tensor approximation ($N_{\max} = 6$), dots – Monte–Carlo simulation results which were not used for the approximation. Figure a – absolute value of resultant force, N; Figure b – absolute value of the resultant moment, $N \cdot m$. The whole surface is specular.

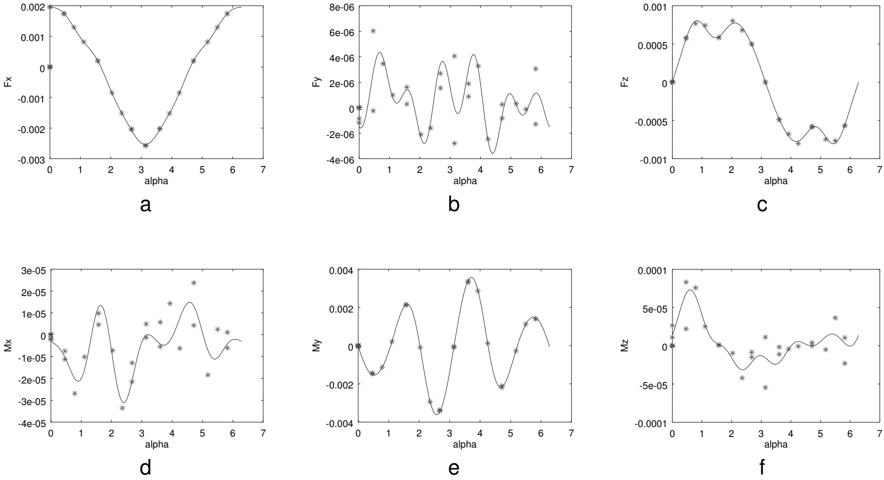

Figure 13: Approximation results ($N_{\max} = 6$) for principal force (a, c, e), N, and for principal moment (b, c, f), $N \cdot m$, of light radiation pressure depending on angle of rotation of light source in the plane of radiators (solid line) comparing results of Monte–Carlo simulations (dots). The results in subfigures b, c, and f are non-zero because of random noise. The dotted values were not used in the construction of approximation. Specular case.

Diffuse case

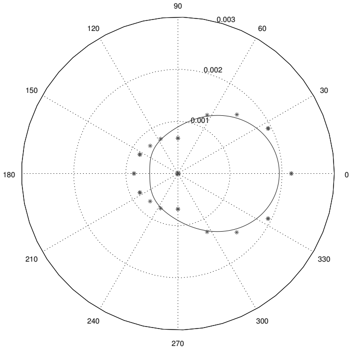

a

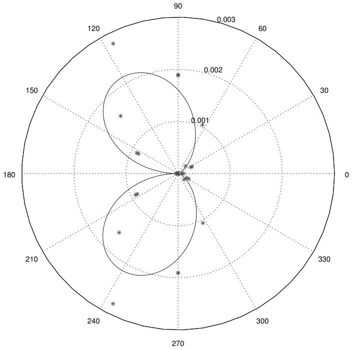

b

Figure 14: Dependency of the absolute value of resultant force and moment of light radiation pressure from the angle of rotation of light source in the radiators plane. Solid line – tensor approximation ($N_{\max} = 2$), dots – Monte–Carlo simulation results which were not used for the approximation. Figure a – absolute value of resultant force, N; Figure b – absolute value of the resultant moment, $N \cdot m$. The whole surface is diffuse.

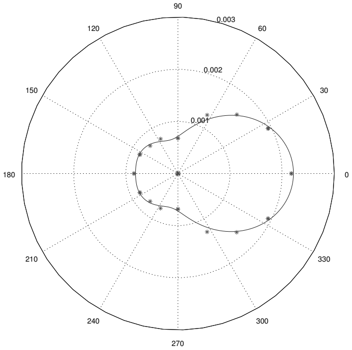

a

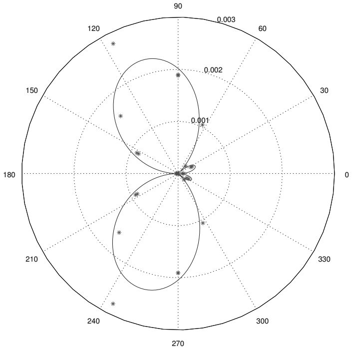

b

Figure 15: Dependency of the absolute value of resultant force and moment of light radiation pressure from the angle of rotation of light source in the radiators plane. Solid line – tensor approximation ($N_{\max} = 3$), dots – Monte–Carlo simulation results which were not used for the approximation. Figure a – absolute value of resultant force, N; Figure b – absolute value of the resultant moment, $N \cdot m$. The whole surface is diffuse.

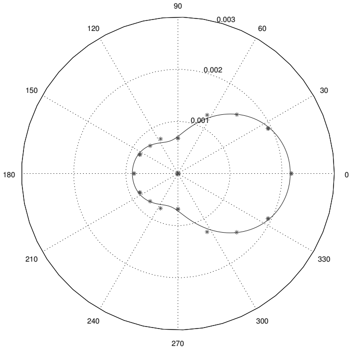

a

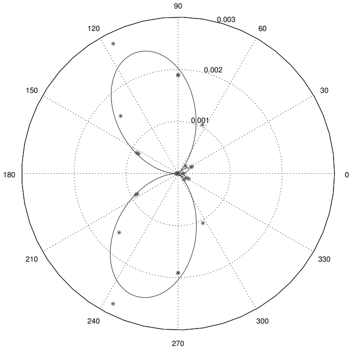

b

Figure 16: Dependency of the absolute value of resultant force and moment of light radiation pressure from the angle of rotation of light source in the radiators plane. Solid line – tensor approximation ($N_{\max} = 4$), dots – Monte–Carlo simulation results which were not used for the approximation. Figure a – absolute value of resultant force, N; Figure b – absolute value of the resultant moment, $N \cdot m$. The whole surface is diffuse.

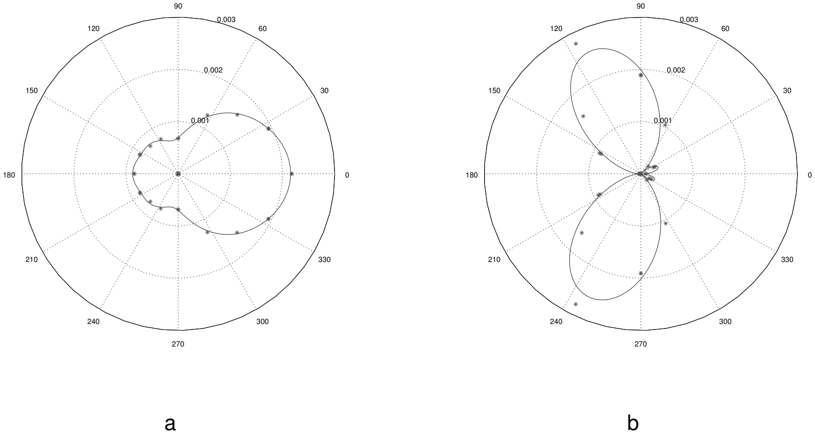

Figure 17: Dependency of the absolute value of resultant force and moment of light radiation pressure from the angle of rotation of light source in the radiators plane. Solid line – tensor approximation ($N_{\max} = 5$), dots – Monte–Carlo simulation results which were not used for the approximation. Figure a – absolute value of resultant force, N; Figure b – absolute value of the resultant moment, $N \cdot m$. The whole surface is diffuse.

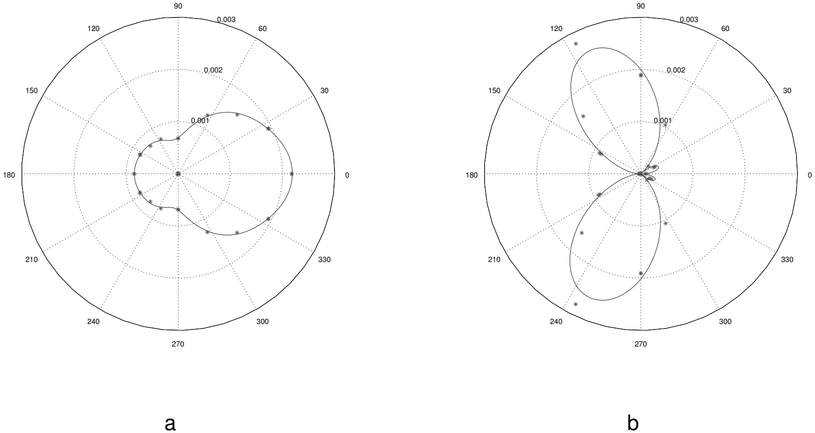

Figure 18: Dependency of the absolute value of resultant force and moment of light radiation pressure from the angle of rotation of light source in the radiators plane. Solid line – tensor approximation ($N_{\max} = 6$), dots – Monte–Carlo simulation results which were not used for the approximation. Figure a – absolute value of resultant force, N; Figure b – absolute value of the resultant moment, $N \cdot m$. The whole surface is diffuse.

Diffuse case, projections

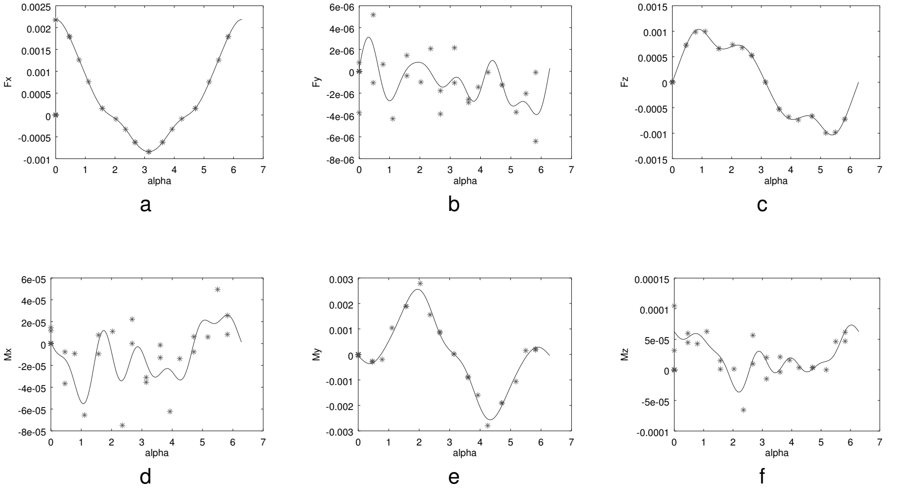

Figure 19: Approximation results ($N_{\max} = 6$) for principal force (a, c, e), N, and for principal moment (b, c, f), $N \cdot m$, of light radiation pressure depending on angle of rotation of light source in the plane of radiators (solid line) comparing results of Monte–Carlo simulations (dots). The results in subfigures b, c, and f are non-zero because of random noise. The dotted values were not used in the construction of approximation. Diffuse case.

Specular-diffuse case

$$\tilde{\mathcal{I}}^1 \approx \tilde{\mathcal{I}}^1|_{s=0} \approx \tilde{\mathcal{I}}^1|_{s=1}; \tag{42}$$

$$\tilde{\mathcal{I}}^2 \approx (1-s)\tilde{\mathcal{I}}^2|_{s=0}; \tag{43}$$

$$\tilde{\mathcal{I}}^3 \approx (1-s)\tilde{\mathcal{I}}^3|_{s=0} + s\tilde{\mathcal{I}}^3|_{s=1}; \tag{44}$$

$$\tilde{\mathcal{I}}^n \approx (1-s)\tilde{\mathcal{I}}^n|_{s=0} + s\tilde{\mathcal{I}}^n|_{s=1}, n > 3; \tag{45}$$

$$\tilde{\mathcal{K}}^1 \approx \tilde{\mathcal{K}}^1|_{s=0} \approx \tilde{\mathcal{K}}^1|_{s=1}; \tag{46}$$

$$\tilde{\mathcal{K}}^2 \approx (1-s)\tilde{\mathcal{K}}^2|_{s=0}; \tag{47}$$

$$\tilde{\mathcal{K}}^n \approx (1-s)\tilde{\mathcal{K}}^n|_{s=0} + s\tilde{\mathcal{K}}^n|_{s=1}, n > 2, \tag{48}$$

Specular–diffuse case, $s = 0.75$

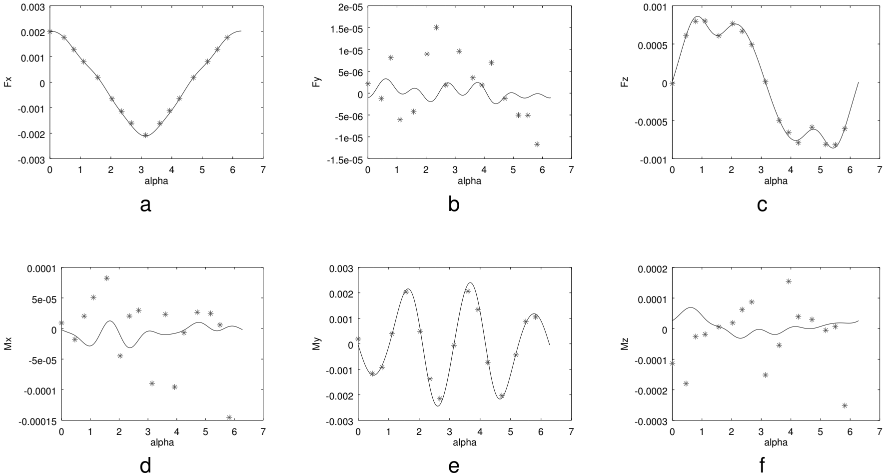

Figure 20: Approximation results ($N_{\max} = 6$) for principal force (a, c, e), N, and for principal moment (b, c, f), $N \cdot m$, of light radiation pressure depending on angle of rotation of light source in the plane of radiators (solid line) comparing results of Monte–Carlo simulations (dots). The results in subfigures b, c and f are non-zero because of random noise. The approximation was constructed as a linear combination of specular and diffuse cases. Specular–diffuse case, $s = 0.75$.

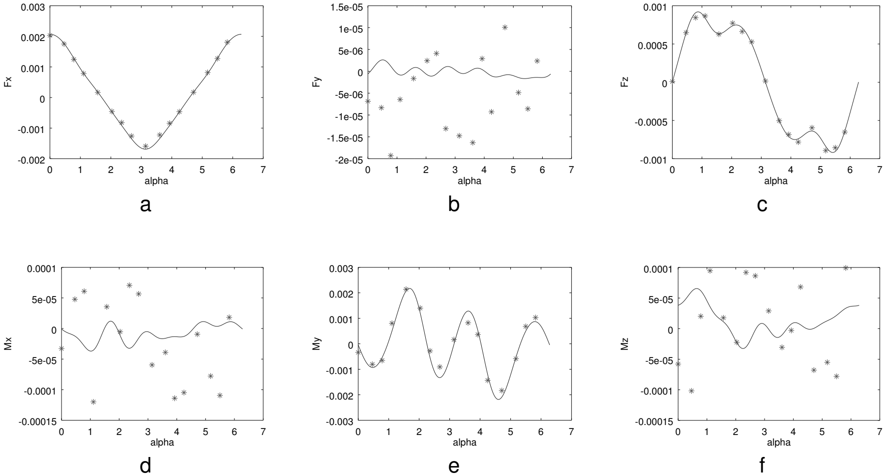

Figure 21: Approximation results ($N_{\max} = 6$) for principal force (a, c, e), N, and for principal moment (b, c, f), $N \cdot m$, of light radiation pressure depending from angle of rotation of light source in the plane of radiators (solid line) comparing results of Monte–Carlo simulations (dots). The results in subfigures b, c and f are non-zero because of random noise. The approximation was constructed as a linear combination of specular and diffuse cases. Specular–diffuse case, $s = 0.5$.

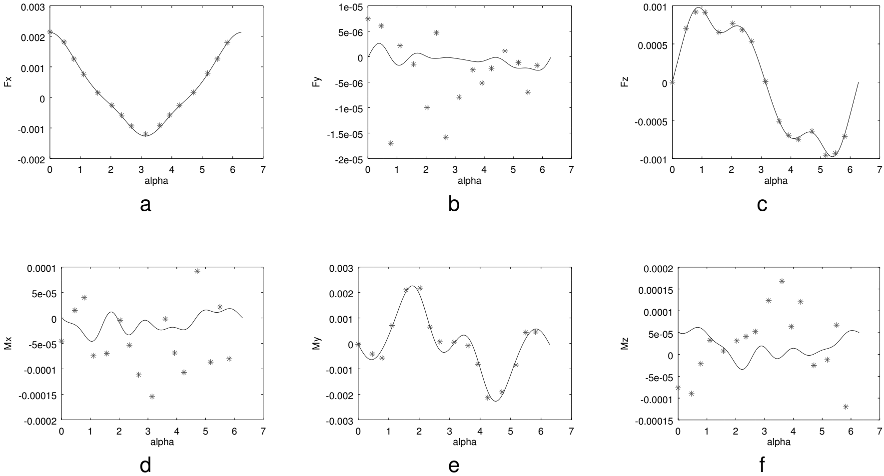

Figure 22: Approximation results ($N_{\max} = 6$) for principal force (a, c, e), N, and for principal moment (b, c, f), $N \cdot m$, of light radiation pressure depending from angle of rotation of light source in the plane of radiators (solid line) comparing results of Monte–Carlo simulations (dots). The results in subfigures b, c and f are non-zero because of random noise. The approximation was constructed as a linear combination of specular and diffuse cases. Specular–diffuse case, $s = 0.25$.

Conclusions and future plans

Conclusions and future plans

Conclusions

- The presented model can describe the SRP of complex space body.
- In the model the geometrical and optical parameters of structure are analytically divided from the attitude towards the sun.
- If the bodies $\mathcal{A}$ and $\mathcal{B}$ are both optically convex, as well as the their composition $\mathcal{A} + \mathcal{B} = \mathcal{C}$, the components of shape tensors for $\mathcal{C}$ can be calculated as a simple sum of corresponding components of shape tensors for $\mathcal{A}$ and $\mathcal{B}$.

Future plans

- Dynamics around the center of inertia under SRP moment. Optimal stabilization law.
- Investigation of connections to the dynamics of the satellites in the upper Earth atmosphere under hyperthermal flow.[4]

[4] Beletskii V., Yanshin A. Vliyanie aerodinamicheskikh sil na vrashchatel'noe dvizhenie iskusstvennykh sputnikov (Effect of the aerodynamic forces on the rotary motion of satellites). Kiev: Naukova Dumka, 1984. P. 187. (in Russian)

Main publications

1. Nerovnyi N, Zimin V (2014) Determination of the radiation pressure force acting on a solar sail taking into account stress-dependent optical parameters of sail material (in Russian). Herald of the Bauman Moscow State Technical University Series Mechanical Engineering 96(3):61–78, URL http://vestnikmach.ru/eng/catalog/simul/hidden/486.html
2. Zimin VN, Nerovnyy NA (2015) Analysis of the deformed shape of a heliogyro solar sail blade taking into account stress-dependent reflectivity of the material (in Russian). Proceedings of Higher Educational Institutions chine Building 658(1):18–23, URL http://izvuzmash.ru/eng/catalog/calcmach/hidden/1125.html
3. Zimin VN, Nerovnyi NA (2016) To the calculation of the main vector and the main momentum of light pressure force on a solar sail (in Russian). Herald of the Bauman Moscow State Technical University Series Mechanical Engineering 106(1):17–28, DOI 10.18698/0236-3941-2016-1-17-28, URL http://vestnikmach.ru/eng/catalog/avroc/airdyn/1055.html
4. Nerovny NA (2017) The resultant vector and principal moment of light radiation pressure upon an optically convex space structure (in Russian). Vestnik St. Petersburg State University Series 1. Mathematics. Mechanics. Astronomy [Approved for publication]
5. Nerovny NA et al. (2017) Representation of light pressure resultant force and moment as a tensor series. Celestial Mechanics and Dynamical Astronomy. [Approved for publication]